Available online at www.sciencedirect.com
ScienceDirect
Journal of Power Sources 162 (2006) 1043–1052
JOURNAL OF POWER SOURCES
www.elsevier.com/locate/jpowsour

Oxygen reduction on strontium-doped $LaMnO_3$ cathodes in the absence and presence of an iron–chromium alloy interconnect

Y.D. Zhen [a], Jian Li [b], San Ping Jiang [a,*]

[a] School of Mechanical and Aerospace Engineering, Nanyang Technological University, 50 Nanyang Avenue, Singapore 639798, Singapore
[b] School of Materials Science and Engineering, Huazhong University of Science and Technology, Wuhan 430074, China

Received 27 May 2006; accepted 20 August 2006
Available online 2 October 2006

Abstract

Oxygen reduction on a Sr-doped $LaMnO_3$ (LSM) electrode of a solid oxide fuel cell (SOFC) is investigated in the absence and the presence of a Fe–Cr alloy interconnect. The results show that oxygen reduction is controlled by a surface exchange reaction that involves dissociative adsorption and diffusion of oxygen on the LSM electrode surface, and migration of oxygen ions from the LSM to the yttria stabilized zirconia (YSZ) electrolyte lattice at the three-phase boundary (TPB). In the presence of Fe–Cr alloy, the reaction order and activation energy of the surface exchange process are similar to those in the absence of Fe–Cr alloy. This indicates that the presence of gaseous chromium species simply reduces the active sites for the surface exchange reaction by blocking oxygen vacancy formation on the LSM electrode surface. On the other hand, the Cr_2O_3/$(Cr,Mn)_3O_4$ solid species deposited on the YSZ electrolyte surface primarily inhibits the migration of oxygen ions into the YSZ electrolyte, as indicated by a significant increase in the activation energy of the migration process of the oxygen ions into YSZ electrolyte.

Keywords: Oxygen reduction; Solid oxide fuel cell; Strontium-doped $LaMnO_3$ cathode; Metallic interconnect; Iron–chromium alloy

1. Introduction

Solid oxide fuel cells (SOFCs) have been extensively investigated as new electricity generation technology because of their high energy-conversion efficiency and low greenhouse gas emissions [1]. Significant progress has been made in lowering the operating temperature of SOFCs to 600–800 °C through significant reduction in electrolyte thickness [2] and the development of new electrode materials [3–5]. A lower operating temperature minimizes the interfacial reaction, increases the stability and reliability of the cell and widens the range of candidate materials for fuel cell components. In particular, a low operating temperature enables the use of metallic interconnect materials for SOFCs [6–10]. Compared with traditional $LaCrO_3$-based ceramic interconnect materials, metals have many advantages that include high thermal and electrical conductivity, negligible ionic conductivity, good machinability, and low cost.

Chromium-containing alloys, especially chromia-forming ferrite stainless steels, are considered to be among the most promising candidates due to their electronically conducting oxide scale and compatible thermal expansion behaviour with other cell components [11]. At high temperatures, however volatile Cr species such as CrO_3 and $Cr(OH)_2O_2$ are generated over the oxide scale layer in oxidizing atmospheres [12,13]. Numerous studies have shown that without an effective protective coating, the gaseous chromium species can cause a serious deterioration of the electrocatalytic activity of Sr-doped $LaMnO_3$ (LSM) for the O_2 reduction reaction [14–20]. There is considerable disagreement over the degradation mechanism of the chromium species on LSM electrodes for O_2 reduction. One theory is that deposition of Cr species at the LSM electrode|YSZ electrolyte interface is limited by electrochemical reduction of gaseous Cr species to solid phase Cr_2O_3 in competition with O_2 reduction [14–18]. Based on this hypothesis, the degradation of LSM electrode performance is closely related to the loss of oxygen activity at the three-phase boundary, TPB, due to deposition of the Cr species. Our systematic studies of Cr deposition processes on various SOFC cathodes such as LSM, $(LaSr)(CoFe)O_3$ and Pt clearly demonstrate that the deposition

* Corresponding author. Tel.: +65 6790 5010; fax: +65 6791 1859.
E-mail address: mspjiang@ntu.edu.sg (S.P. Jiang).

0378-7753/$ – see front matter © 2006 Elsevier B.V. All rights reserved.
doi:10.1016/j.jpowsour.2006.08.034

process of Cr species at a LSM electrode is limited kinetically by chemical dissociation of the high valent Cr species [21–23]. The deposition reaction at the LSM|YSZ interface is most likely controlled by the nucleation and grain growth of Cr species, which are initiated by manganese species (e.g., Mn^{2+}) generated under cathodic polarization or at high temperatures.

The O_2 reduction on a LSM electrode is a complex process even in the absence of a Fe–Cr alloy [24–27]. The reaction is a multi-step process that includes oxygen diffusion within the porous electrode, dissociative adsorption of oxygen species, oxygen surface diffusion to the TPB region, charger transfer, and migration of oxygen ions from the TPB into the YSZ electrolyte. One or several of these steps may be rate-limiting. The exact details of the overall reaction mechanism and kinetics for O_2 reduction are not clearly understood. Thus, it is of scientific importance to investigate and compare the O_2 reduction reaction on a LSM electrode in the presence and the absence of Fe–Cr alloy under identical SOFC operating conditions. In this paper, O_2 reduction reactions on LSM electrodes in the absence and presence of a Fe–Cr alloy interconnect have been studied. The results clearly identify the role of the gaseous and solid Cr species.

2. Experimental details

Zirconia electrolyte discs were prepared from 8 mol% Y_2O_3 doped ZrO_2 powder (YSZ, Tosoh, Japan) by die pressing, followed by sintering at 1500 °C for 4 h in air. The thickness and diameter of the sintered electrolyte were ~1 and 19 mm, respectively. A-site nonstoichiometry $(La_{0.8}Sr_{0.2})_{0.9}MnO_3$ (LSM) powders were synthesized by co-precipitation and calcined at 1000 °C in air. The LSM cathode coating was applied to a YSZ electrolyte by screen-printing and sintered at 1150 °C for 2 h in air. The electrode area was 0.5 cm^2. Platinum paste (Ferro Corporation, USA) was painted on the opposite side of the LSM electrode to serve as the counter and reference electrodes. The counter electrode was symmetrical to the LSM electrode and the reference electrode was painted as a ring around the counter electrode.

A commercial Fe–Cr alloy RA446 (Rolled Alloy Co., Canada) was machined into coupons (12 mm × 12 mm × 4 mm in size). Channels (1.2 mm × 1.2 mm) were cut on one side of each coupon. Air was directed to the channels through an alumina tube. Two Pt wires were spot-welded to the coupon to serve as voltage and current probes, respectively. There was no Pt mesh placed between the chromia-forming alloy and the electrode coating. Air (industrial grade, H_2O content <3 ppm, SOXAL) was dried through a molecular sieve before use. The air flow rate was 100 mL min^{-1}. The cell configuration and the arrangement of the Fe–Cr alloy interconnect have been reported elsewhere [23]. For experiments in the absence of Fe–Cr alloy, a Pt mesh served as the current-collector for the LSM electrodes. A separate and Cr-free sample holder was used in order to avoid the Cr contamination.

The polarization behaviour of LSM electrodes in the absence and the presence of Fe–Cr alloy was examined at a constant current density of 200 mA cm^{-2} in air at 900 °C. The polarization potential ($E_{Cathode}$) was measured against the Pt air reference electrode. The current was interrupted from time to time to undertaken electrochemical impedance spectroscopy (EIS) measurements. A Solartron 1260 frequency response analyzer in conjunction with a 1287 electrochemical interface was used to perform EIS measurements in the frequency range of 0.1–100 kHz. The measurements were made at open-circuit and under a cathodic dc bias. In the latter case, a continuous cathodic current of 200 mA cm^{-2} was passed to the LSM electrode by means of an external galvanostatic–potentiostatic generator (Hokuto Denko HAB-151). The impedance responses were analyzed by the equivalent circuit method. The electrode ohmic resistance (R_Ω) was measured from the high-frequency intercept and the electrode interface (polarization) resistance (R_E) was directly obtained from the difference between the high- and low-frequency intercepts on the impedance spectra. The overpotential (η) was calculated from $E_{Cathode}$ and R_Ω by the following equation.

$$E_{Cathode} = \eta + jR_\Omega \quad (1)$$

where j is the current density.

The O_2 reduction reaction in the absence and presence of a Fe–Cr alloy was studied in the temperature range of 900–750 °C and at an oxygen partial pressure between 0.01 and 1 atm. In the absence of Fe–Cr alloy, LSM electrodes were polarized at 900 °C and 200 mA cm^{-2} prior to measurement in order to stabilize the electrode. In the presence of Fe–Cr alloy, the EIS measurements were conducted on a LSM electrode after polarization at 900 °C and 200 mA cm^{-2} for 45 h.

Scanning electron microscopy (SEM, Leica 360) and X-ray energy dispersion spectroscopy (EDS, Oxford) were used to examine the morphology of the LSM|YSZ interface. In order to examine the YSZ electrolyte surface in contact with the LSM electrode coating, the LSM electrode was removed by 20% HCl acid treatment, followed by washing with de-ionized water. Details of the Cr deposition in the LSM|YSZ system have been reported previously [21,23].

3. Results and discussion

3.1. Impedance behaviour at open-circuit

Fig. 1 shows the initial impedance responses of LSM electrodes as a function of cathodic current passage of 200 mA cm^{-2} at 900 °C in the absence and presence of Fe–Cr alloy. The EIS was measured at open-circuit. For O_2 reduction in the absence of a Fe–Cr alloy (Fig. 1(a)), the initial R_E is 2.11 Ω cm^2, and reduces significantly with the passage of current. The rapid reduction in R_E indicates the significant activation effect of cathodic polarization on the electrochemical activity of a freshly prepared LSM electrode for O_2 reduction [28–30]. The activation effect of the cathodic polarization on the initial electrode behaviour of the LSM electrode is also observed in the presence of Fe–Cr alloy, as shown in Fig. 1(b). In the presence of Fe–Cr alloy, however, the decrease in the impedance appears to be slower, as compared with that in the absence of Fe–Cr alloy. The reduction in the elec-

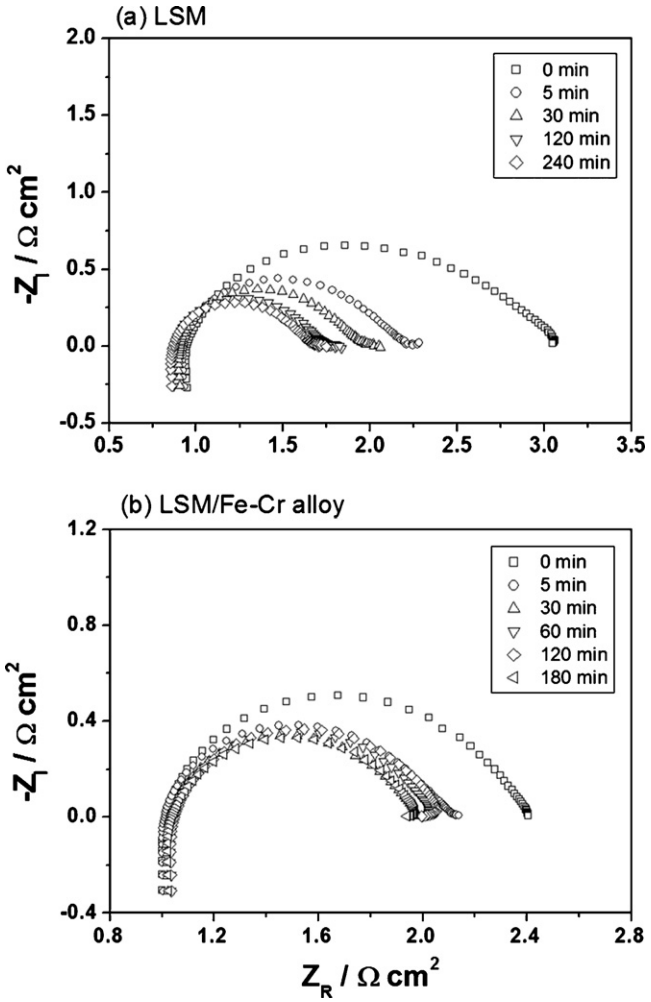

Fig. 1. Initial impedance responses of LSM electrodes as function of a cathodic current passage of 200 mA cm^{-2} in (a) absence and (b) presence of Fe–Cr alloy at 900 °C. EIS is measured at open-circuit.

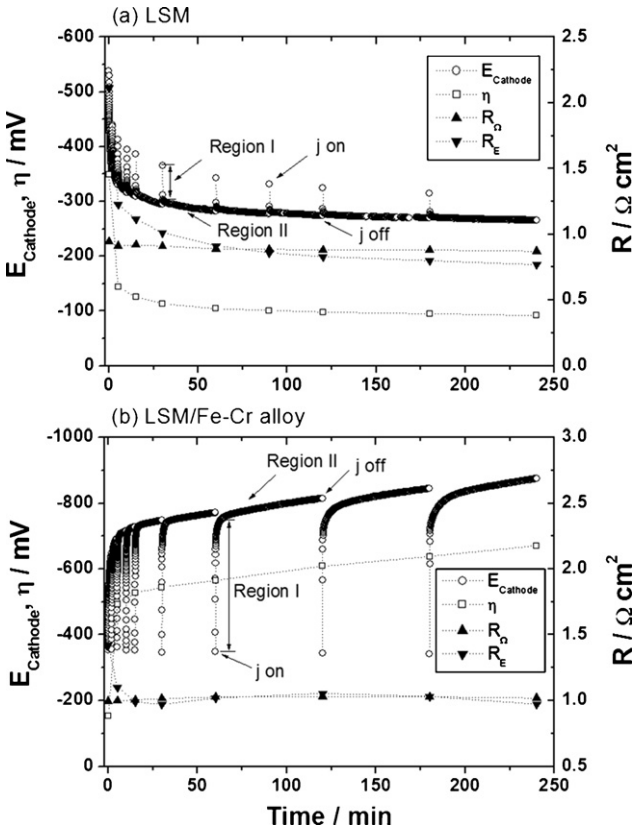

Fig. 2. Initial polarization curves of LSM electrodes as function of a cathodic current passage of 200 mA cm^{-2} in (a) absence and (b) presence of Fe–Cr alloy at 900 °C. The electrode polarization and ohmic resistances (R_E and R_Ω) are taken from the impedance spectra of Fig. 1.

trode polarization resistance for O_2 reduction in the presence of Fe–Cr alloy has also been reported by Matsuzaki and Yasuda [16].

Fig. 2 shows the initial polarization curves of the LSM electrodes as a function of the passage of a cathodic current of 200 mA cm^{-2} at 900 °C in the absence and presence of Fe–Cr alloy. The polarization behaviour is characterized by two distinct regions. The polarization behaviour of the LSM electrode in the absence of Fe–Cr alloy is very different to that in the presence of Fe–Cr alloy. In the absence of Fe–Cr alloy, $E_{Cathode}$ decreases rapidly (region I), and these follows a region in which the decrease in $E_{Cathode}$ is much slower (region II). The significant decrease of the polarization potential confirms the activation effect of cathodic polarization on the LSM electrodes. In the presence of Fe–Cr alloy, instead of a rapid decrease, $E_{Cathode}$ increases very quickly in region I, but is much slower in the following region II. As R_Ω remains almost constant with the passage of current, the increase or decrease in $E_{Cathode}$ is due mainly to a change in η. The significant difference in the change of $E_{Cathode}$ in the absence and presence of Fe–Cr alloy indicates the strong inhibiting effect of Cr species on O_2 reduction. Unlike the increase in η, the R_E measured at open-circuit in the presence of Fe–Cr alloy does not change significantly with on passing a cathodic current.

3.2. Impedance behaviour under dc bias

The oxygen reduction reaction was also studied under dc bias in the absence and presence of Fe–Cr alloy. Fig. 3 shows the initial impedance and polarization potential responses for O_2 reduction on a LSM electrode in the absence of Fe–Cr alloy under a continuous cathodic current of 200 mA cm^{-2} at 900 °C. The EIS was measured under a dc bias. The impedance responses of LSM electrodes are characterized by an overlapped and depressed arc and exhibit an inductive loop at low frequencies. The latter has also been reported for O_2 reduction on a LSM porous electrode [31] and on a LSM point electrode [32] under a dc bias. For the O_2 reduction on a LSM electrode in the absence of a Fe–Cr alloy, the impedance is reduced significantly on passing cathodic current (Fig. 3(a)). The decrease of R_E is consistent with the decrease of $E_{Cathode}$, as shown in Fig. 3(b).

The impedance and polarization potential responses of a LSM electrode in the presence of Fe–Cr alloy under a continuous cathodic current of 200 mA cm^{-2} at 900 °C is given in Fig. 4. The EIS was measured under a dc bias. The impedance responses for O_2 reduction in the presence of Fe–Cr alloy are also characterized by an overlapped and depressed arc. As opposed to

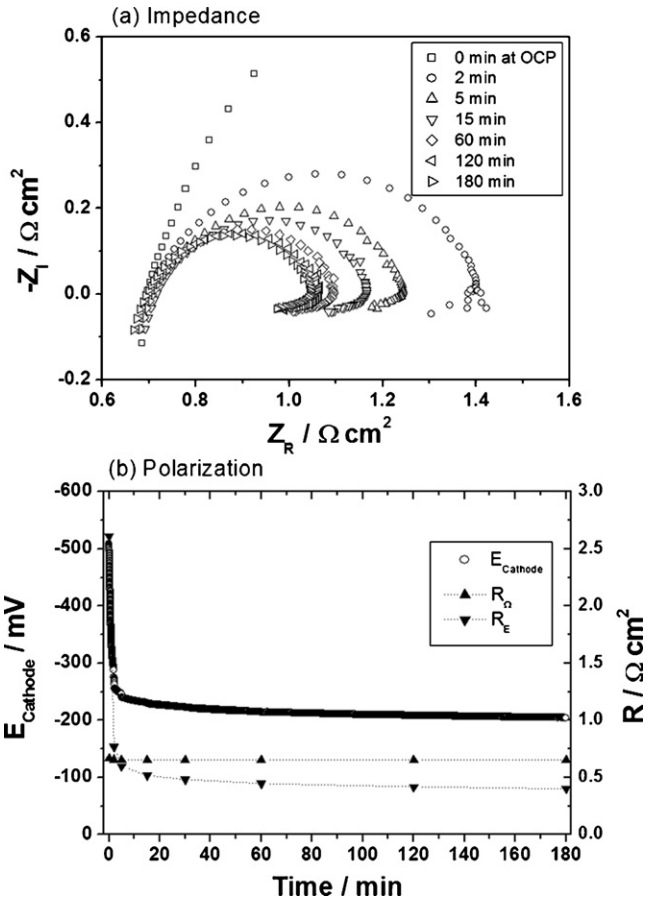

Fig. 3. (a) Nyquist plots and (b) polarization potential curves of LSM electrode for O_2 reduction in absence of Fe–Cr alloy at 900 °C as a function of a cathodic current passage of 200 mA cm^{-2}. EIS is measured under dc bias.

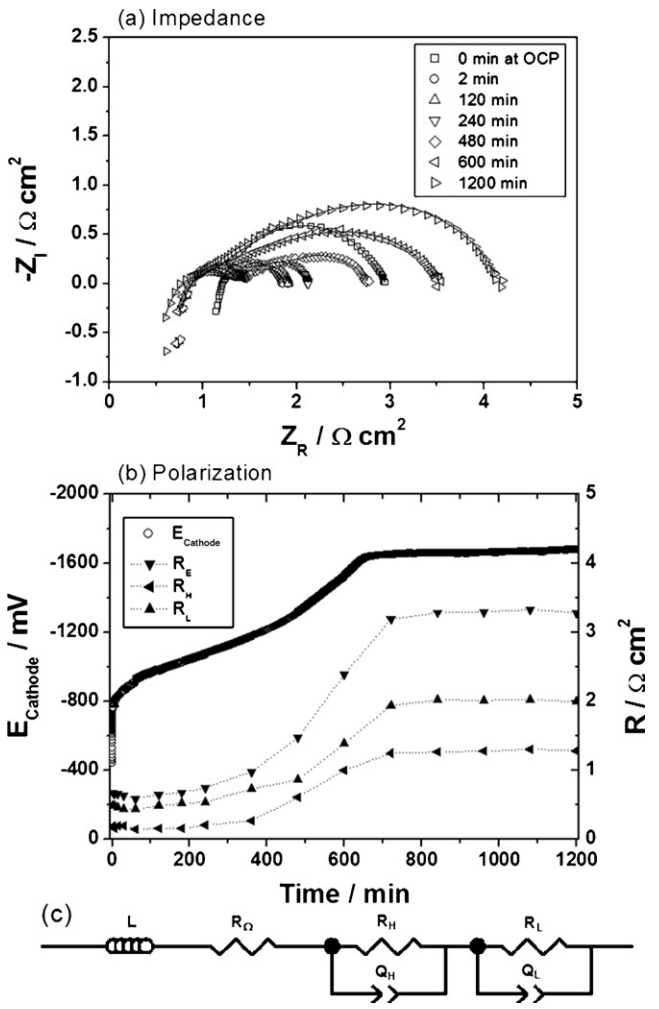

Fig. 4. (a) Nyquist plots and (b) polarization potential curves of LSM electrode for O_2 reduction in presence of Fe–Cr alloy at 900 °C as function of cathodic current passage of 200 mA cm^{-2}. EIS is measured under dc bias. The equivalent circuit is shown in (c). Symbols are measured data, while lines are fitted results.

the behaviour in the absence of Fe–Cr alloy, there are no inductance loops at low frequencies. In general, both R_E and $E_{Cathode}$ increase with cathodic current passage. After a continuous current for about 600 min, the increases in $E_{Cathode}$ and R_E become much smaller. The R_E is 3.27 Ω cm^2 after 1200 min, which is significantly higher than the initial R_E of 0.68 Ω cm^2. The equivalent circuit, which is composed of two (R–Q) circuits in series (e.g., $L\,R_\Omega(R_HQ_H)(R_LQ_L)$), was used for the fitting (Fig. 4(c)). In the circuit, L, Q and R denote the inductance, the constant phase element and the electrode resistance, respectively. R_Ω is the ohmic resistance between the cathode and the reference electrode. Subscripts H and L correspond to the high and low frequency arcs. In Fig. 4, the symbols are experimental data and the solid lines are the fitting results. The match of the equivalent circuit to the experimental data is quite reasonable (Fig. 4(a)).

Impedance responses measured under the cathodic current of 200 mA cm^{-2} and at open-circuit immediately after the interruption of the cathodic current passage at 900 °C are presented in Fig. 5. The LSM electrode was polarized for 3 h in the absence of Fe–Cr alloy and for 20 h in the presence of Fe–Cr alloy, respectively. For O_2 reduction in the absence of Fe–Cr alloy, the impedance arc increases after the interruption of the cathodic current. It is found that R_E changes from 0.35 Ω cm^2 under a dc bias to 0.72 Ω cm^2 at open-circuit. The inductive loop at low frequencies under a dc bias becomes capacitive loop after removal of the dc bias (Fig. 5(a)). This shows that the inductive loop at low frequencies only occurs under bias. This is consistent with that reported for O_2 reduction on porous and pin-shaped LSM electrodes [31,32].

By contrast, for O_2 reduction in the presence of Fe–Cr alloy, the impedance arc decreases significantly after the removal of the cathodic polarization. The R_E decreases quickly from 3.38 to 0.69 Ω cm^2 after interruption of the cathodic current (Fig. 5(b)). There is also a significant change in the characteristics of the impedance responses before and after the switching off the catholic current. The impedance responses at open-circuit in the presence of Fe–Cr alloy can be clearly separated at low and high frequencies. On the other hand, the impedance responses for O_2 reduction in the presence of Fe–Cr alloy measured under bias are characterized by a straight line at high frequencies (Fig. 5(b)), which indicate a finite-length Warburg impedance [33]. When the penetration depth of the concentration perturbation ($\lambda = (2D/\omega)$) is small in comparison with the width of the diffusion layer (δ), the Warburg impedance can be represented

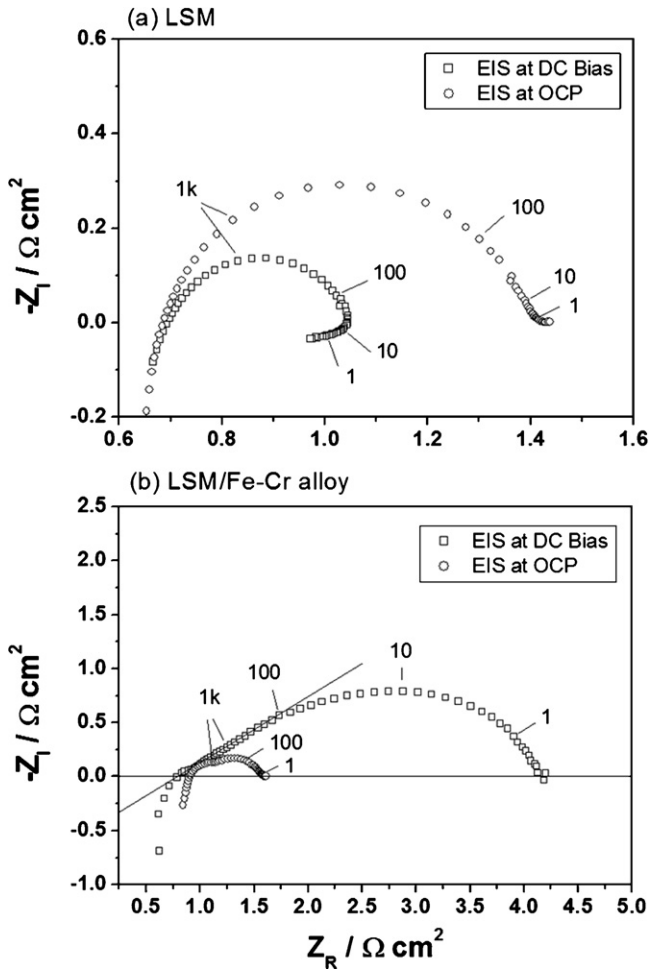

Fig. 5. Impedance responses of LSM electrodes for O_2 reduction reaction at 900 °C under cathodic polarization of 200 mA cm^{-2} and at open-circuit immediately after interruption of cathodic polarization in (a) absence and (b) presence of Fe–Cr alloy. The LSM electrode was polarized for 3 h in absence of Fe–Cr alloy, and for 20 h in presence of a Fe–Cr alloy, respectively, before the interruption of cathodic current.

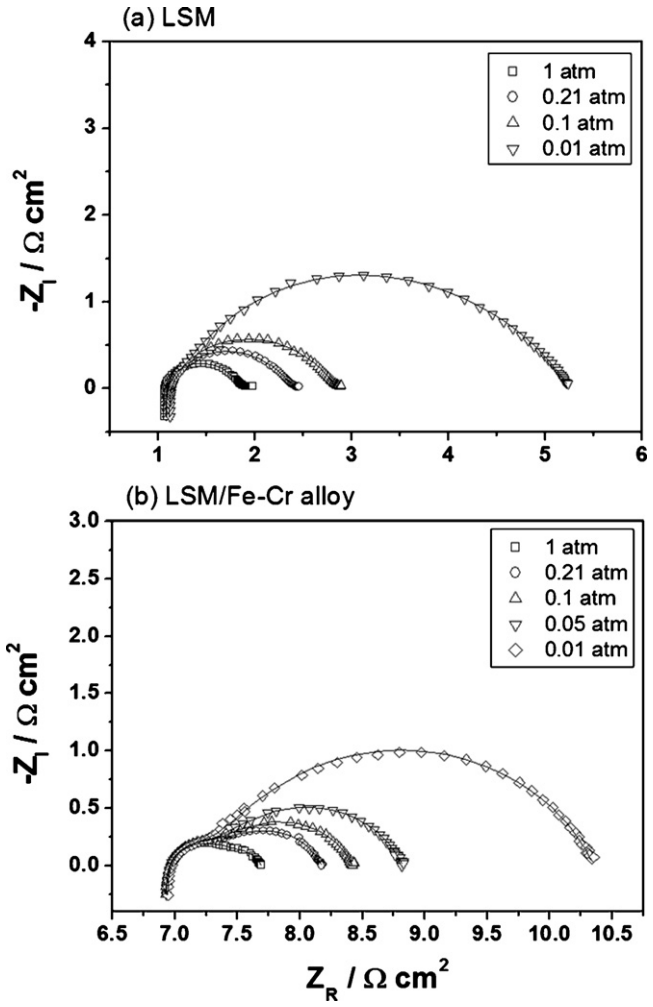

Fig. 6. Impedance curves of LSM electrodes for O_2 reduction in (a) absence and (b) presence of Fe–Cr alloy as function of oxygen partial pressure at 900 °C. LSM electrode in presence of Fe–Cr alloy is polarized at 200 mA cm^{-2} for 45 h before impedance measurement. EIS is measured at open-circuit.

by a straight line making an angle of 45° with the real axis, and the diffusion occurs in an effectively semi-infinite medium. This is most likely due to the deposition of the Cr species at the YSZ|electrolyte surface, which slows the rate of the migration of the oxygen ions from the three-phase boundary into YSZ electrolyte lattice [19]. As shown below for O_2 reduction in the presence of Fe–Cr alloy, there is a formation of dense Cr deposits at the LSM|YSZ interface. For reaction on a porous LSM electrode in the presence of Fe–Cr alloy, the angle of the straight line with the real axis is ∼32°, i.e., smaller than 45°. This may indicate the complicated diffusion process of oxygen species in the presence of solid Cr deposits.

3.3. Reaction order and activation energy

The impedance responses of LSM electrodes measured at open-circuit and 900 °C in the absence and presence of Fe–Cr alloy as a function of the partial pressure of oxygen are given in Fig. 6. LSM electrodes were polarized for 4 and 45 h at 200 mA cm^{-2} in the absence and presence of Fe–Cr alloy, respectively, prior to the EIS measurement at open-circuit. The symbols are the experimental data and lines are the fitted results based on the equivalent circuit of Fig. 4(c). The size of the impedance arcs increase with decrease in the oxygen partial pressure and the change occurs primarily at low frequencies. Table 1 gives an example of the impedance parameters evaluated by the equivalent circuit for O_2 reduction on a LSM electrode in the absence and presence of a Fe–Cr alloy in air. The data show that, the frequency power (n) for the low- and high-frequency arcs varies between 0.65 and 0.85, i.e., significantly below unity. This implies that the Q is not a pure capacitance [33]. The rate for the electrode processes associated with the low and high frequency arcs (RQ) decrease in comparison with those in the absence of Fe–Cr alloy.

Plots of the P_{O_2}-dependence of the electrode interface conductivity of the electrode processes at the high- and low-frequency arcs ($\sigma_H = 1/R_H$ and $\sigma_L = 1/R_L$) are given in Fig. 7 for O_2 reduction on LSM electrodes in the absence and presence of a Fe–Cr alloy at 900 °C. The electrode process associated

Table 1
Impedance parameters evaluated from equivalent circuit for O_2 reduction on LSM electrode in absence and presence of Fe–Cr alloy at 900 °C in air

Electrode	High-frequency arc				Low-frequency arc			
	R_H (Ω cm^2)	Q_H (Ω^{-1} cm^{-2} s^n)	n	RQ (s^n)	R_L (Ω cm^2)	Q_L (Ω^{-1} cm^{-2} s^n)	n	RQ (s^n)
LSM	0.67	2.5×10^{-3}	0.85	1.68×10^{-3}	0.69	2.6×10^{-2}	0.60	1.79×10^{-2}
LSM/Fe–Cr alloy	0.47	1.5×10^{-3}	0.72	7.05×10^{-4}	0.80	8.7×10^{-3}	0.75	6.96×10^{-3}

Impedance curves for reaction on LSM/Fe–Cr alloy cell measured under open-circuit after polarization at 200 mA cm^{-2} for 45 h.

with the high-frequency arc (σ_H) is independent of P_{O_2}. On the other hand, the reaction order of the electrode process of the low-frequency arc (σ_L) is 0.58 with respect to P_{O_2} in the absence of Fe–Cr alloy, and very close to 0.55 in the presence of Fe–Cr alloy. The impedance responses were also measured at different temperatures and fitted by equivalent-circuit analysis. The reaction orders of the low- and high-frequency electrode processes are listed in Table 2 with respect to P_{O_2} measured at different temperatures. The reaction order of σ_H is independent of P_{O_2} and temperature, regardless of the absence or presence of Fe–Cr alloy. In the absence of Fe–Cr alloy, however, the reaction order of σ_L with respect to P_{O_2} is 0.49 ± 0.07 and does not change significantly within the temperature range studied. This value is close to that reported for LSM electrodes by other authors [25,32,34]. Similar behaviour for the reaction order for σ_L in the presence of a Fe–Cr alloy was also observed and the reaction order is 0.62 ± 0.09, i.e., slightly higher than that in the absence of Fe–Cr alloy. This indicates that the presence of Fe–Cr alloy does not affect significantly the reaction order of the electrode process for O_2 reduction on a LSM electrode.

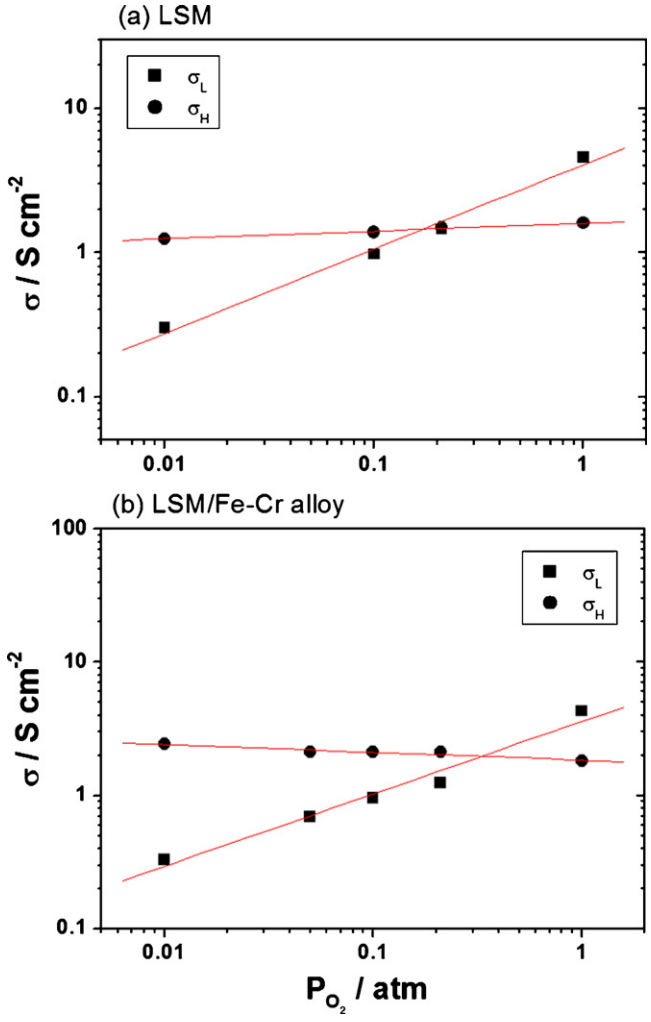

Fig. 7. Plots of electrode conductivity of electrode processes at high- and low-frequency arcs of LSM electrodes in (a) absence and (b) presence of Fe–Cr alloy at 900 °C.

The activation energy plots of the electrode conductivity of high- and low-frequency arcs of LSM electrodes in the absence and presence of Fe–Cr alloy in air are shown in Fig. 8. For O_2 reduction on a LSM electrode in the absence of Fe–Cr alloy, the activation energy of σ_L is 142 kJ mol^{-1} while that of σ_H is 95 kJ mol^{-1}. The activation energy of ~95 kJ mol^{-1} for the electrode process at high-frequency is close to that of the conductivity of a YSZ electrolyte [35]. For O_2 reduction in the presence of Fe–Cr alloy, the activation energy of σ_L is 153 kJ mol^{-1}, i.e., close to that found in the absence of Fe–Cr alloy. On the other hand, the activation energy of σ_H increases significantly to 167 kJ mol^{-1}. The high activation energy for the electrode process associated with the high-frequency arc in the presence of Fe–Cr alloy was also found in our earlier study of O_2 reduction on a LSM electrode/3 mol% Y_2O_3–ZrO_2 electrolyte system [19]. This shows that in the presence of Fe–Cr alloy, O_2 reduction at the high-frequency arc becomes much slower due to the deposition of the Cr species on the YSZ electrolyte surface.

3.4. Microstructure of the LSM electrodes

Scanning electron micrographs of LSM electrodes in the absence of Fe–Cr alloy after a cathodic polarization for 4 h and in the presence of a Fe–Cr alloy for 20 h at 900 °C are presented in Fig. 9. For the O_2 reduction in the absence of Fe–Cr alloy, well-defined and granular-shaped particles with clear grain

Table 2
Reaction order with respect to oxygen partial pressure for electrode processes at high- and low-frequency arcs at different temperatures in absence and presence of Fe–Cr alloy interconnect in air

Temperature (°C)	Reaction order, x in $P_{O_2}^x$			
	LSM		LSM/Fe–Cr alloy	
	σ_H	σ_L	σ_H	σ_L
900	0.05	0.58	−0.05	0.55
850	0.09	0.51	0.15	0.55
800	0.02	0.45	0.05	0.72
750	0.10	0.46	0.11	0.68

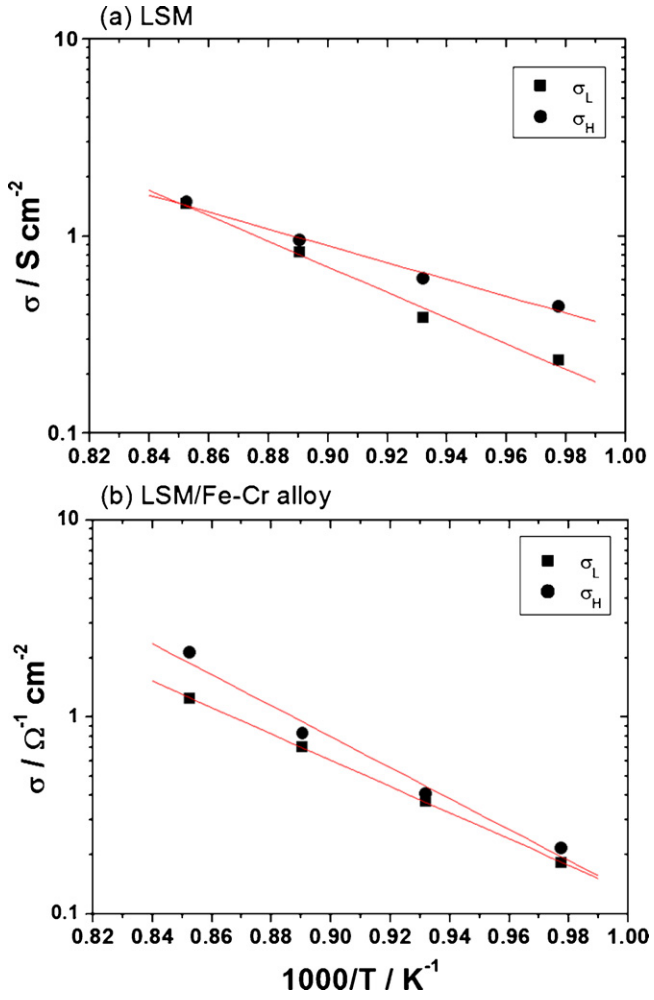

Fig. 8. Activation energy plots of electrode conductivity of high- and high-frequency arcs for O_2 reduction on LSM electrodes in absence and presence of Fe–Cr alloy in air.

boundaries are observed (Fig. 9(a and c)). The size of the LSM grains is in the range of 0.5–1.2 μm. The YSZ electrolyte surface in contact with LSM electrode is clear after the LSM electrode coating is removed by HCl acid treatment. The convex rings formed during the electrode sintering steps are contact areas between the LSM grains and the YSZ electrolyte surface [36] (Fig. 9(e)).

After passage of cathodic current at 200 mA cm^{-2} and 900 °C for 20 h in the presence of Fe–Cr alloy, the surface and bulk of the LSM electrode appear clean with no visible Cr deposition (Fig. 9(b and d)), i.e., similar to that in the absence of Fe–Cr alloy. There is, however significant Cr deposition at the LSM electrode|YSZ electrolyte interface, as indicated by the formation of crystals with well-defined facets (Fig. 9(d)). After the acid etching of the LSM electrode coating, the Cr species deposits are clearly visible on the YSZ electrolyte surface. The space between the LSM grains (indicated by the contact rings) on the YSZ electrolyte surface is almost covered by Cr deposits (Fig. 9(f)). EDS analysis of the deposits reveals the existence of Cr and Mn, which indicates that the crystals are $(Cr,Mn)_3O_4$ spinels [23]. Thus, after cathodic polarization at 200 mA cm^{-2} and 900 °C for 20 h, dense Cr deposits are formed at the LSM electrode and in the YSZ electrolyte surface region.

Table 3
Polarization and impedance behaviour for the O_2 reduction on LSM electrodes in absence and presence of Fe–Cr alloy

LSM	LSM/Fe–Cr alloy
$E_{Cathode}$ decreases with cathodic current passage	$E_{Cathode}$ increases with cathodic current passage
R_E at open-circuit decreases with polarization time	R_E at open-circuit decreases with polarization time
R_E at dc bias decreases with polarization time: $R_H > R_L$	R_E at dc bias increases with polarization time: $R_H < R_L$
$R_{E,dc\ bias} < R_{E,OCP}$	$R_{E,dc\ bias} > R_{E,OCP}$
$R_H \propto P^0_{O_2}$ for T = 900–750 °C	$R_H \propto P^0_{O_2}$ for T = 900–750 °C
$R_L \propto P^{0.49}_{O_2}$ for T = 900–750 °C	$R_L \propto P^{0.62}_{O_2}$ for T = 900–750 °C
$E_{a,R_H} = 95\ kJ\ mol^{-1}$	$E_{a,R_H} = 167\ kJ\ mol^{-1}$
$E_{a,R_L} = 142\ kJ\ mol^{-1}$	$E_{a,R_L} = 153\ kJ\ mol^{-1}$

3.5. Effect of Cr species on reaction mechanism

The polarization and impedance responses for O_2 reduction in the absence and presence of Fe–Cr alloy measured under similar SOFC operating conditions are listed in Table 3. In the absence of Fe–Cr alloy, the polarization potential decreases significantly with the passage of cathodic current due to the activation effect. In the presence of Fe–Cr alloy, however, the polarization potential increases very rapidly with cathodic current and such performance deterioration is nearly reproducible at the early stage of the reaction (Fig. 2), which indicates the dominant inhibiting effect of gaseous Cr species on O_2 reduction.

The impedance behaviour of O_2 reduction in the absence and presence of Fe–Cr alloy indicates that the reaction is broadly controlled by two reaction steps namely, a surface exchange step and migration (i.e., the diffusion) of the oxygen species from the TPB into YSZ electrolyte lattice. This is general consistent with common consensus for the mechanism and kinetics of oxygen reduction on LSM electrodes [20,24–27,31,32,37]. The reaction order of ~0.5 with respect to the P_{O_2} for the electrode process associated with low-frequency arc indicates that the surface exchange step probably involves atomic oxygen species [38]. The high activation energy of σ_L (~142 kJ mol^{-1}) shows that the diffusion of the atomic oxygen species most likely occurs through the surface sites, e.g., the oxygen vacancy sites, on the LSM surface because gaseous diffusion through the pores would require a much smaller activation energy. Thus, the steps for the surface exchange process associated with the low-frequency arc in the impedance spectra can be written as:

$$\tfrac{1}{2}O_2(g) + V^{\bullet\bullet}_{O,LSM} \rightarrow O_{ad,LSM} \quad (2)$$

$$O_{ad,LSM} \rightarrow O_{ad,LSM(TPB)} \quad (3)$$

$$O_{ad,LSM(TPB)} + 2e \rightarrow O^{2-}_{LSM(TPB)} \quad (4)$$

where $V^{\bullet\bullet}_O$ stands for an oxygen vacancy, and the subscripts denote an oxygen vacancy in the LSM electrode lattice or the YSZ electrolyte lattice. $O_{ad,\ LSM}$ is an oxygen species that occupies an active site on the LSM electrode surface. The indepen-

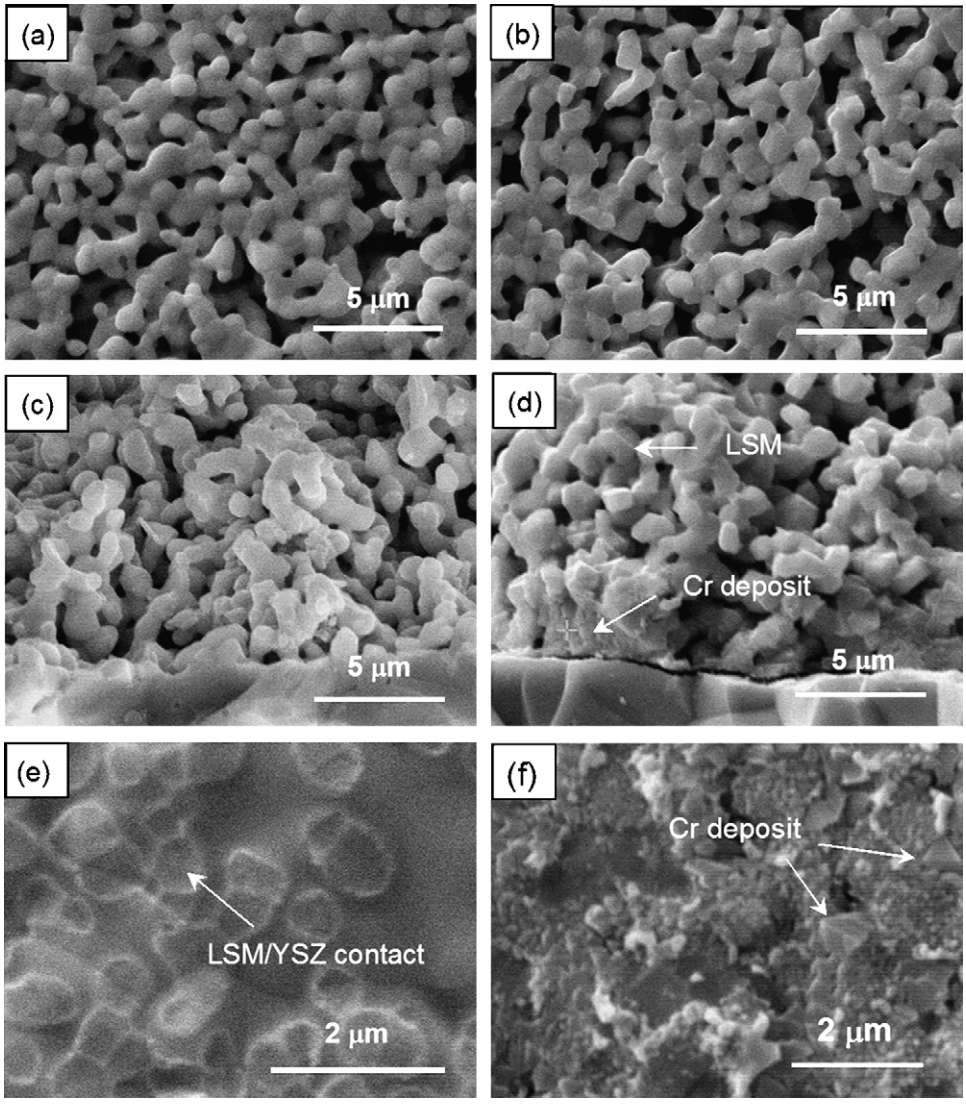

Fig. 9. Scaning electron micrographs of LSM electrode after cathodic current passage at 200 mA cm^{-2} and 900 °C in the absence of Fe–Cr alloy for 4 h (a, c, e) and in presence of Fe–Cr alloy for 20 h (b, d, f). (a) and (b) surface of LSM electrode; (c) and (d) LSM electrode|YSZ electrolyte interface; (e) and (f) YSZ electrolyte surface in contact with LSM electrode. LSM electrode coating removed by HCl acid treatment.

dence of the reaction order and activation energy of the surface exchange step for O_2 reduction in the presence of Fe–Cr alloy is probably due to the fact that Cr species are not preferentially deposited on the LSM surface [22,23]. Thus, the inhibiting effect of gaseous Cr species on the surface diffusion process would be most effective under polarization.

It has been shown that under high cathodic polarization potentials, oxygen vacancies are generated at the LSM electrode surface [26,39], and result in delocalization of the reaction sites and a significant increase in the surface exchange process on the LSM electrode surface. This is supported by the significant reduction in R_E and $E_{Cathode}$ for the O_2 reduction in the absence of Fe–Cr alloy. In the presence of Fe–Cr alloy, however, the gaseous Cr species may inhibit the formation of oxygen vacancies on the LSM electrode surface under cathodic polarization, thus increasing significantly the resistance for the surface exchange process of oxygen. This is supported by an instantaneous increase in the polarization potential with passage of cathodic current and an increase in R_E under dc bias (Figs. 2 and 4). As the effect of gaseous Cr species is primarily to reduce the active sites on the LSM electrode surface, the reaction order and activation energy of the electrode process of the surface exchange step would be similar to that in the absence of Fe–Cr alloy. This is the observation made in the present study.

The electrode process at the high-frequency arc is characterized by a zero reaction order with respect to P_{O_2} and an activation energy of about ~95 kJ mol^{-1} for O_2 reduction in the absence of Fe–Cr alloy on a LSM electrode. The zero reaction order suggests that neither atomic oxygen nor molecular oxygen are involved in the reaction step. A recent investigation of O_2 reduction on porous LSM electrodes shows that R_H is basically independent of dc bias [37]. This indicates that the electrode process at the high-frequency arc cannot be associated with a charge-transfer process. The similarity in frequency power (n) and reaction rate (RQ) of the high- and low-frequency electrode processes (Table 1) indicates that the electrode process asso-

ciated with the high-frequency arc is also a diffusion process. Therefore, the high-frequency arc most likely corresponds to the migration and diffusion of oxygen ions from the TPB regions into the YSZ lattice, which can be expressed as:

$$O^{2-}_{LSM(TPB)} \rightarrow O^{2-}_{YSZ(TPB)} + V^{\bullet\bullet}{}_{O,LSM} \quad (5)$$

The activation energy of the above process is ~95 kJ mol^{-1}, i.e., close to that of the ionic conductivity of YSZ electrolyte materials [35]. Uchida et al. [40] found that the electrode performance of LSM electrodes increases with ionic conductivity of the zirconia electrolyte in the temperature range of 800–1000 °C. Adding a ceria interlayer has also been shown to reduce significantly the interfacial resistance at the LSM cathodes [41]. This indicates that the transport of oxygen ions into the electrolyte would be promoted by an increase in the ionic conductivity of the electrolyte.

As shown in Fig. 9, dense and thick Cr deposits, i.e., Cr_2O_3 and $(Cr,Mn)_3O_4$ spinels, are formed at the LSM|YSZ interface after cathodic current passage of 200 mA cm^{-2} for 20 h at 900 °C. Thus, the migration and transfer process of oxygen ions would have to proceed through a dense and thick Cr species layer formed on the YSZ electrolyte surface before entering the YSZ electrolyte lattice. It is well-known that chromium oxide is a very poor conductor of oxygen ions. The oxygen self-diffusion coefficient in Cr_2O_3 single crystals is ~10^{-18} cm^2 s^{-1} at 1100 °C [42] and in Cr_2O_3 polycrystals is ~10^{-13} cm^2 s^{-1} at 1100 °C [43], i.e., significantly lower than 10^{-8} to 10^{-7} cm^2 s^{-2} at 900 °C reported for YSZ electrolytes [44,45]. Therefore, the migration of oxygen ions into the electrolyte will be dominated by the diffusion of oxygen through the solid Cr_2O_3 and $(Cr,Mn)_3O_4$ deposit layer, and will cause a significant increase in electrode resistance to the migration of oxygen ions into the YSZ electrolyte. This is indicated by a marked increase in R_H with the passage of cathodic current in comparison with R_L (Fig. 4). The high activation energy of ~167 kJ mol^{-1} of R_H in the presence of Fe–Cr alloy is most likely associated with the high activation energy of ~230 kJ mol^{-1} for oxygen diffusion in Cr_2O_3 [42]. Therefore, for O_2 reduction in the presence of Fe–Cr alloy where a solid Cr deposit layer is formed on the YSZ electrolyte surface, the oxygen migration process (reaction (5)) will proceed according to [19]:

$$O^{2-}_{LSM,TPB} \rightarrow O^{2-}_{Cr_2O_3/(Cr,Mn)_3O_4,TPB} + V^{\bullet\bullet}{}_{O,LSM} \quad (6)$$

$$O^{2-}_{Cr_2O_3/(Cr,Mn)_3O_4,TPB} \rightarrow O^{2-}_{YSZ} \quad (7)$$

where $O^{2-}_{Cr_2O_3/(Cr,Mn)_3O_4,TPB}$ is an oxygen ion in the $Cr_2O_3/(Cr,Mn)_3O_4$ oxide lattice or at an interstitial site close to the TPB region.

At low frequencies, an inductive loop under a dc bias moves to a capacitive loop at open-circuit for O_2 reduction in the absence of Fe–Cr alloy (Fig. 5). The fact that there is no inductive loop in the presence of Fe–Cr alloy suggests that the inductive loop for O_2 reduction on a LSM electrode under a dc bias in the absence of Fe–Cr alloy is not related to possible 'crosstalk' between the working and the reference electrodes [46,47]. The inductive loop under a dc bias has been ascribed [48] to the onset of mixed conductivity in the electrolyte due to the direct injection of electron holes in the YSZ. Van Hassel et al. [49,50] also observed an inductive loop at low frequencies under a bias for O_2 reduction on a porous gold electrode on YSZ. From detailed model analysis the inductive loop was explained in terms of two adsorbed species competing for adsorption sites. Such an explanation could also apply to O_2 reduction on porous LSM electrodes under cathodic polarization.

4. Conclusions

The effect of Fe–Cr alloy on oxygen reaction taking place on a Sr-doped $LaMnO_3$ (LSM) electrode of solid oxide fuel cells (SOFCs) has been investigated. The reaction process is controlled by a surface exchange reaction that comprises the dissociative adsorption and diffusion of oxygen on the LSM surface, and the migration of oxygen ions from the three-phase boundary (TPB) to the YSZ electrolyte lattice. In the presence of a Fe–Cr alloy interconnect, the surface exchange processes shows a zero reaction order with respect to oxygen partial pressure and the activation energy is 153 kJ mol^{-1}, which is similar to that of the reaction in the absence of Fe–Cr alloy. This indicates that gaseous Cr species reduce the number of active sites on the LSM electrode surface for the surface-exchange step. The deposition of Cr species at the YSZ electrolyte surface physically block the migration of oxygen ions from LSM to the YSZ electrolyte lattice, which results in a significantly slow electrode step associated with a high frequency arc. This is indicated by a significantly increased activation energy (~167 kJ mol^{-1}). The inhibiting effect of Cr deposits on the overall O_2 reduction reaction becomes increasingly dominant with cathodic polarization time.

Acknowledgement

Y.D. Zhen thanks the Nanyang Technological University for a research student scholarship.

References

[1] N.Q. Minh, T. Takahashi, Science and Technology of Ceramic Fuel Cells, Elsevier, Amsterdam, 1995.
[2] L.C. De Jonghe, C.P. Jacobson, S.J. Visco, Annu. Rev. Mater. Res. 33 (2003) 169.
[3] S.P. Jiang, S. Zhang, Y.D. Zhen, A.P. Koh, Electrochem. Solid-State Lett. 7 (2004) A282.
[4] E.P. Murray, T. Tsai, S.A. Barnett, Nature 400 (1999) 649.
[5] S.P. Jiang, Mater. Sci. Eng. A 418 (2006) 199.
[6] W.Z. Zhu, S.C. Deevi, Mater. Res. Bull. 38 (2003) 957.
[7] K. Huang, P.Y. Hou, J.B. Goodenough, Solid State Ionics 129 (2000) 237.
[8] T. Horita, Y. Xiong, K. Yamaji, N. Sakai, H. Yokokawa, J. Electrochem. Soc. 150 (2003) A243.
[9] T. Brylewski, M. Nanko, T. Maruyama, K. Przybylski, Solid State Ionics 143 (2001) 131.
[10] Z. Yang, K.S. Weil, D.M. Paxton, J.W. Stevenson, J. Electrochem. Soc. 150 (2003) A1188.
[11] J.W. Fergus, Mater. Sci. Eng. A 397 (2005) 271.
[12] K. Hilpert, D. Das, M. Miller, D.H. Peck, R. Weiβ, J. Electrochem. Soc. 143 (1996) 3642.
[13] H.G. Graham, H.H. Davis, J. Electrochem. Soc. 54 (1971) 89.

[14] S. Taniguchi, M. Kadowaki, H. Kawamura, T. Yasuo, Y. Akiyama, Y. Miyake, T. Saitoh, J. Power Sources 55 (1995) 73.
[15] S.P.S. Badwal, R. Deller, K. Foger, Y. Ramprakash, J.P. Zhang, Solid State Ionics 99 (1997) 297.
[16] Y. Matsuzaki, I. Yasuda, Solid State Ionics 132 (2000) 271.
[17] K. Fujita, T. Hasimoto, K. Ogasawara, H. Kameda, Y. Matsuzaki, T. Sakurai, J. Power Sources 131 (2004) 270.
[18] Y. Matsuzaki, I. Yasuda, J. Electrochem. Soc. 148 (2001) A126.
[19] S.P. Jiang, J.P. Zhang, K. Foger, J. Electrochem. Soc. 147 (2000) 3195.
[20] S.P. Jiang, J. Appl. Electrochem. 31 (2001) 181.
[21] S.P. Jiang, J.P. Zhang, L. Apateanu, K. Foger, J. Electrochem. Soc. 147 (2000) 4013.
[22] S.P. Jiang, J.P. Zhang, X.G. Zheng, J. Eur. Ceram. Soc. 22 (2002) 361.
[23] S.P. Jiang, S. Zhang, Y.D. Zhen, J. Mater. Res. 20 (2005) 747.
[24] J.-D. Kim, G.-D. Kim, J.-W. Moon, Y.-i. Park, W.-H. Lee, K. Kobayashi, M. Nagai, C.-E. Kim, Solid State Ionics 143 (2001) 379.
[25] S. Wang, Y. Jiang, Y. Zhang, J. Yan, W. Li, J. Electrochem. Soc. 145 (1998) 1932.
[26] H.Y. Lee, W.S. Cho, S.M. Oh, H.D. Wiemhofer, W. Gopel, J. Electrochem. Soc. 142 (1995) 2659.
[27] X.J. Chen, K.A. Khor, S.H. Chan, J. Power Sources 123 (2003) 17.
[28] W. Wang, S.P. Jiang, Solid State Ionics 177 (2006) 1361.
[29] S.P. Jiang, L.G. Love, Solid State Ionics 158 (2003) 45.
[30] S.P. Jiang, L.G. Love, Solid State Ionics 138 (2001) 183.
[31] B. Gharbage, T. Pagnier, A. Hammou, J. Electrochem. Soc. 141 (1994) 2118.
[32] E. Siebert, A. Hammouche, M. Kleitz, Electrochim. Acta 40 (1995) 1741.
[33] S.P. Jiang, J.G. Love, S.P.S. Badwal, Key Eng. Mater. 125–126 (1997) 81.
[34] S.P. Jiang, J.G. Love, Y. Ramprakash, J. Power Sources 110 (2002) 201.
[35] F.T. Ciacchi, K.M. Crane, S.P.S. Badwal, Solid State Ionics 73 (1994) 49.
[36] S.P. Jiang, W. Wang, Electrochem. Solid-State Lett. 8 (2005) A115.
[37] S.P. Jiang, Solid State Ionics 146 (2002) 1.
[38] Y. Takeda, R. Kanno, M. Noda, Y. Tomida, O. Yamamoto, J. Electrochem. Soc. 134 (1987) 2656.
[39] T. Horita, K. Yamaji, M. Ishikawa, N. sakai, H. Yokokawa, T. Kawada, T. Kato, J. Electrochem. Soc. 145 (1998) 3196.
[40] H. Uchida, M. Yoshida, M. Watanabe, J. Electrochem. Soc. 146 (1999) 1.
[41] T. Tsai, S.A. Barnett, Solid State Ionics 98 (1997) 191.
[42] A.C.S. Sabioni, A.M. Huntz, F. Millot, C. Monty, Philos. Mag. A 66 (1992) 351.
[43] A.C.S. Sabioni, A.M. Huntz, F. Millot, C. Monty, Philos. Mag. A 66 (1992) 361.
[44] L.A. Simpson, R.E. Carter, J. Am. Ceram. Soc. 49 (1966) 139.
[45] K. Park, D.R. Olander, J. Electrochem. Soc. 138 (1992) 1154.
[46] B.A. Boukamp, Solid State Ionics 143 (2001) 47.
[47] G. Fafilek, Solid State Ionics 176 (2005) 2023.
[48] E.J.L. Schouler, M. Kleitz, J. Electrochem. Soc. 134 (1987) 1045.
[49] B.A. van Hassel, B.A. Boukamp, A.J. Burggraaf, Solid State Ionics 48 (1991) 139.
[50] B.A. van Hassel, B.A. Boukamp, A.J. Burggraaf, Solid State Ionics 48 (1991) 155.